

Experimental Test of Gravitationally Induced Quantum Interference*

A. W. Overhauser and R. Colella

Department of Physics, Purdue University, West Lafayette, Indiana 47907

(Received 25 July 1974)

We call attention to a feasible laboratory experiment with an outcome that depends necessarily on both Planck's constant and the gravitational constant. A neutron interferometer for which the two beams enclose an area of $\sim 6 \text{ cm}^2$ can be cut from a single crystal of silicon. A shift of ~ 10 fringes is anticipated when the interferometer is rotated 180° about an axis parallel to both the earth's surface and the incident neutron beam.

The technical development of x-ray interferometers¹ (made possible by the availability of large dislocation-free crystals of Si) suggests a variety of studies involving thermal-neutron interferometry.² A particularly interesting and fundamental application juxtaposes gravity and quantum mechanics.

A schematic drawing of a neutron interferometer is shown in Fig. 1. The three shaded slabs are part of (and extend out from) a single crystal of Si. A small angular fraction (0.17 sec of arc) of the incident neutron beam follows the upper path $ABCEF$. A similar fraction follows the lower path $ABDEF$. The two beams are coherent and are intercepted by a small He^3 counter at F . On account of angular divergence most of the incident beam cannot undergo a Bragg reflection and so passes through the instrument along the line AD . A quantitative analysis of these factors based on the dynamical theory of diffraction is reported below.

Our calculation of the anticipated interference effect is based on the Hamiltonian

$$H = p^2/2M + Mgy, \quad (1)$$

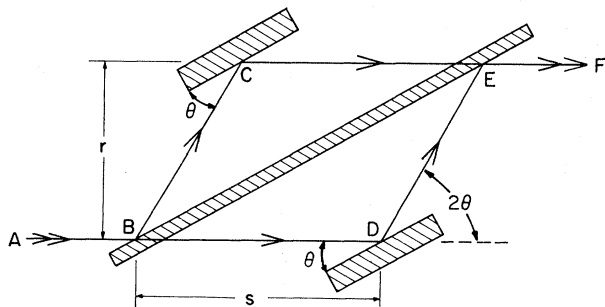


FIG. 1. Schematic illustration of a neutron interferometer. The neutron beams are Bragg reflected at B , C , D , and E by protruding slabs (shaded) of a single crystal of Si. θ is the Bragg angle.

where M is the neutron mass, g the acceleration of gravity, and y the vertical height. We assume that the Newtonian potential Mgy is appropriate for a thermal neutron. The free fall of neutrons has been measured⁴ and agrees with Eq. (1), as one expects from the correspondence principle.

There are several possible contributions to the quantum-mechanical phase difference between the lower and upper paths of Fig. 1. Suppose at the outset that the paths are exactly given by the parallelogram in Fig. 1. Then at any instant the phase lengths for the path segments BC and DE will be equal. However the phase difference for the segment BD will exceed that for CE by

$$\Delta\varphi = s\Delta k, \quad (2)$$

where the wave-vector difference Δk arises from the difference in height r of these segments:

$$\Delta k \cong 2\pi M^2 g r \lambda / h^2, \quad (3)$$

where λ is the wavelength of the neutron and h is Planck's constant.

Another contribution could arise because the ray BD will strike the reflecting planes at D at an angle $\theta + \delta$ instead of θ . The (very small) deviation δ is caused by the gravitational acceleration of the neutrons during the time, s/v , of their travel from B to D .

$$\delta \cong gs/v^2 \sim 3 \times 10^{-8}, \quad (4)$$

where v is the neutron velocity. As a consequence, the direction of the Bragg-reflected ray DE will be $2\theta + \delta$ instead of 2θ (with respect to the horizontal). A ray leaving D with a direction $2\theta + \delta$ will reflect off the beam splitter at a point E' (instead of E , Fig. 1) which is displaced downwards along the surface (towards B). This displacement causes the length of the ray between these points of reflection to be reduced by

$$\Delta L' \cong 2r\delta \cos\theta / \sin^2(2\theta) \sim 10 \text{ \AA}. \quad (5)$$

However one can show (by symmetry about the reflection surface) that the phase of the horizontal ray passing through the beam splitter at E' will correspond (at that point) to an equal reduction in length $\Delta L'$ relative to a ray at E . As a consequence there will be no contribution (to first order in g) from this effect to the interference.

A similar path distortion occurs because the ray BC arrives at C at a Bragg angle $\theta - \epsilon$ instead of θ , with

$$\epsilon = gr \cos(2\theta)/v^2 \sin(2\theta). \quad (6)$$

The ray CE will then have an angle ϵ above the horizontal. Consequently it will emerge from the beam splitter at a point E'' (instead of E), which is displaced upwards *along the surface* by an amount

$$\Delta L'' \cong 2s\epsilon \cos\theta/\sin(2\theta). \quad (7)$$

However the ray from (near) D which reflects at E'' will have a phase (at E'') equivalent to an increased length $\Delta L''$. Again there will be no contribution to the interference.

Shifts of the reflection points C , D , and E caused by the gravitational distortion of the rays into parabolas are also $\sim 10 \text{ \AA}$ and lead to phase changes that cancel to first order in g .

The total phase difference between the two paths is that given by Eqs. (2) and (3). If the interferometer is rotated about the axis AD , the relative roles of the alternate paths are interchanged. Consequently the total fringe shift ΔN will be twice $\Delta\phi/2\pi$:

$$\Delta N = 2M^2 grs\lambda/h^2. \quad (8)$$

Even if the neutron λ is expressed in terms of its classical momentum, the fringe shift ΔN still depends on the ratio g/h . ΔN is proportional to the area, rs , enclosed by the two paths. If this area is 6 cm^2 and $\lambda = 1.42 \text{ \AA}$, the expected fringe shift is $\Delta N = 10.7$.

Elastic distortion of the interferometer during the 180° rotation will contribute a shift of about 1 fringe. This can be measured independently by repeating the experiment with x rays. Design of an interferometer that will function for both neutrons and x rays involves a compromise on the thickness of the beam splitter (slab BE of Fig. 1). We have found a suitable design based on the use of 0.71-\AA ($\text{Mo } K\alpha$) x rays and 1.42-\AA neutrons. Similar beam paths result when the former undergo (440) and the latter (220) Bragg reflections.

Theoretical performance of our design has been computed⁵ by using the dynamical theory appro-

priate¹ to an interferometer of the type shown in Fig. 1. The beam splitter was taken to be 1 mm thick. To optimize x-ray transmission the reflecting planes form an angle of 8° with the surface of the beam splitter. The integrated intensity⁶ (for x rays) at F , when the two beams interfere constructively, is 2.3×10^{-8} . Since the dynamical index of refraction for x rays differs from unity by $\sim 5 \times 10^{-6}$, it follows that the crystal surfaces must be smooth to $\sim \pm 10^{-4} \text{ cm}$ over the areas where the beams interact with the crystal. This condition is not difficult to achieve.

For the case of two 1.42-\AA neutron beams interfering constructively, the integrated intensity is 2.5×10^{-7} . With neutron beams currently available at high-flux reactors, the counting rate at the detector should be tens of counts per second. The dynamic index of refraction for neutrons differs from unity by $\sim 10^{-7}$. Consequently the requirements on surface flatness are less stringent ($\sim \pm 50 \times 10^{-4} \text{ cm}$) than that for x rays.

We conclude that the proposed experiment is feasible. It is not obvious (to us) that all conceivable theories of gravitation will lead to the fringe shift, Eq. (8),⁷ predicted by a scalar Newtonian potential. An experimental result in disagreement with Eq. (10) would question the validity of the principle of equivalence⁸ in the quantum limit. Agreement could of course be regarded as a check of the equivalence principle away from the classical limit, $\hbar \rightarrow 0$.

*Work supported in part by the National Science Foundation under Contract No. GH 41884.

¹U. Bonse and M. Hart, Z. Phys. **194**, 1 (1966).

²Successful construction of a neutron interferometer has been reported recently: H. Rauch, W. Treimer, and U. Bonse, Phys. Lett. **47A**, 369 (1974).

³The central peak of the Bragg reflection (which has a Darwin width of 0.5 sec) is totally reflected at B , C , and E and emerges from the interferometer along a line parallel to DE . The rocking curve of the interferometer consists of two 0.08-sec wide peaks separated by the 0.5-sec Darwin gap.

⁴A. W. McReynolds, Phys. Rev. **83**, 172 (1951); J. W. T. Dabbs, J. A. Harvey, D. Paya, and H. Horstmann, Phys. Rev. **139**, B756 (1965).

⁵The existence of multiply reflected beams within the beam splitter has been neglected. For the case of neutrons these may have appreciable intensity because absorption is small. They can be eliminated (for narrow beams) by suitable shielding. An important point in the theory (Ref. 1) is that the phase difference between the two beams at F does not depend on the precise angle of incidence (within the 0.2-sec angular window). This implies that the incident wave at A can be spheri-

cal.

⁶Unit integrated intensity is defined to be 100% of the incident beam arriving at the detector throughout an angular rotation of the crystal of 1 rad.

⁷We emphasize that Eq. (8) applies to an interferometer for which the beam splitter is very thin. Rays are refracted as they enter and leave the beam splitter (near *B* and *E*). Phase differences caused by this phe-

nomenon could not arise were the angle $\epsilon - \delta$, given by Eqs. (4) and (6), equal to zero. Since $\epsilon - \delta \sim 10^{-8}$, a small correction to Eq. (8) may result for a beam splitter of finite thickness, depending on design.

⁸Equation (8) can also be derived when no gravitational field is present provided the nuclear reactor, beam port, etc., and the interferometer have a uniform acceleration g .

Multiplicity Distributions and Multiplicity Scaling in $p + p \rightarrow p + \text{MM}$ at 28.5 GeV/c*

T. S. Clifford,† A. R. Erwin, J. R. Ficenc, G. P. Larson, E. Lazarus, K. M. Moy,
W. N. Schreiner,† P. Schübelin, W. P. Trower, and F. Turkot

Brookhaven National Laboratory, Upton, New York 11973, and Virginia Polytechnic Institute and State University, Blacksburg, Virginia 24061, and University of Wisconsin, Madison, Wisconsin 53706

(Received 27 August 1974)

The charged particles associated with a fast forward trigger proton of four-momentum transfer t in the reaction $p + p \rightarrow p + \text{MM}$ at 28.5 GeV/c were measured using the Multiparticle Argo Spectrometer System. Charged-particle multiplicity distributions show multiplicity scaling with respect to the missing mass, MM, to $\sim 10\%$ within each of two t regions, $0 < |t| < 2$ (GeV/c)² and $3 < |t| < 5$ (GeV/c)². The width of the scaling curve shrinks between regions.

We previously reported the behavior of the average number of charged particles, $\langle n_c \rangle$, produced in the reaction

$$p_1 + p_2 \rightarrow p_3 + \text{MM} \quad (1)$$

at 28.5 GeV/c.¹ We observed a sharp rise in $\langle n_c \rangle$ with increasing t , the four-momentum transfer from p_1 to p_3 , for fixed mass MM recoiling against p_3 . Here we describe certain regularities in the shapes of the charge multiplicity distributions, $P_{n_c}(\text{MM}, t)$, and examine the scaling properties in MM and t and their correlation with the rise in $\langle n_c \rangle$. Such observations may be helpful in understanding the dynamical mechanism of particle production in high-energy pp collisions.

Our data base consists of $\sim 200\,000$ events of Reaction (1). The data were taken at Brookhaven National Laboratory by the Multiparticle Argo Spectrometer System (MASS).² The high-momentum spectrometer (HMS) momentum analyzed and identified p_3 , and the vertex spectrometer (VS)³ momentum analyzed the remaining charged particles. The VS tracks were reconstructed by the computer code PITRACK⁴ and fitted to a common vertex. Corrections were applied¹ to the multiplicity distributions to compensate for loss of charged particles due to limited solid angle ($\sim 10\%$), low-momentum cutoff ($\sim 1\%$), and software inefficiencies ($\sim 6\%$).

The probability for a given charged multiplicity

associated with a trigger proton of given MM and t is

$$P_{n_c}(\text{MM}, t) \equiv \frac{d^2 \sigma_{n_c} / d(\text{MM}) dt}{\sum_i d^2 \sigma_i / d(\text{MM}) dt} \quad (2)$$

The data, which cover the range $1.2 < \text{MM} < 6.5$ GeV and $0.2 < |t| < 6.5$ (GeV/c)², have been divided into 31 bins of MM and t by taking six intervals in MM and seven in t . For each bin we calculated the average charged multiplicity in the final state, $\langle n_c \rangle$, the dispersion, $D^2 \equiv \langle n_c^2 \rangle - \langle n_c \rangle^2$, and two higher normalized moments, $C_i \equiv \langle n_c^i \rangle / \langle n_c \rangle^i$, $i = 3, 4$, of $P_{n_c}(\text{MM}, t)$; the results are given in Table I. In analyzing the data with finer binning⁵ one sees that for fixed MM > 2 GeV, the average charge multiplicity is approximately constant for $|t| < 2$ (GeV/c)², then rises abruptly by $\Delta n_c \sim 0.6$ charged particles and again becomes approximately constant for $|t| > 3$ (GeV/c)². This constancy of $\langle n_c \rangle$ for fixed MM in the two t regions is also observed⁵ in the individual P_{n_c} . The magnitude of the increase and the t value at which it is centered are approximately constant for all intervals of MM > 2 GeV. We found that the rise is centered at $|t| \sim 2.5$ (GeV/c)² and occurs in a characteristic interval $\Delta t \sim 1$ (GeV/c)².

Figure 1 is a plot of $P_{n_c}(\text{MM}, t)$ versus MM averaged over two t intervals on either side of the rise in $\langle n_c \rangle$: Region I has $1 < |t| < 2$ (GeV/c)² and region II has $3 < |t| < 5$ (GeV/c)². Compari-